Photodiagnosis and Photodynamic Therapy 26 (2019) 448–454

Contents lists available at ScienceDirect

Photodiagnosis and Photodynamic Therapy

journal homepage: www.elsevier.com/locate/pdpdt

Novel half-sandwich rhodium(III) and iridium(III) photosensitizers for dual chemo- and photodynamic therapy

Wei Su[a], Zhijin Luo[a], Shuai Dong[c], Xiufeng Chen[a], Jun-an Xiao[a], Binghua Peng[a], Peiyuan Li[b,*]

[a] Key Laboratory of Guangxi Key Laboratory of Natural Polymer Chemistry and Physics (Nanning Normal University), Nanning, China
[b] College of Pharmacy, Guangxi University of Chinese Medicine, Nanning, China
[c] Chongqing Insistute of Forensic Science, Chongqing, China

ARTICLE INFO

Keywords:
Half-sandwich complexes
Dual action
Chemodynamic
Photodynamic therapy

ABSTRACT

Background and objective: Photodynamic therapy has emerged as a promising treatment for cancer and other malignancies. Design of photosensitizers with two different action mechanisms may be an essential strategy for the improvement of the efficacy of phototherapeutic drugs. The objective of this study was to evaluate the anticancer photo- and chemocytotoxic effects of the novel half-sandwich rhodium(III) and iridium(III) photosensitizers.

Materials and methods: A series of novel half-sandwich Cp*-Rh(III) and Cp*-Ir(III) complexes containing 9-anthraldehyde thiosemicarbazones, (Cp*)M(L)Cl (M = Rh or Ir, L = 9-anthraldehyde thiosemicarbazones), were compared for cell uptake and photo- and chemocytotoxic effects against human prostate carcinoma (PC3) and human ovarian carcinoma (SKOV3) cell lines.

Results: Cp*-Ir(III) complexes, (Cp*)Ir(L)Cl, showed remarkable phototoxic behavior against human ovarian adenocarcinoma SKOV3 cells (IC_{50} = 2.7 and 2.3 μM, respectively, λ_{irr} > 400 nm), as well as the 7.4 and 5.3-fold lower toxicity in the dark, implying possibility of dual action as chemo- and phototherapeutic agents.

Conclusion: The complexes, which present a synergistic effect with good properties of both the Cp*-Rh(III) and Cp*-Ir(III) chemotherapeutic effect and the anthracene photodynamic therapy efficiency, show great potential as a new generation of light activated dual-action anticancer agents for photodynamic therapy.

1. Introduction

Photodynamic therapy, as a complementary methodology to common current anticancer therapies, has emerged as a promising treatment for cancer and other malignancies. The use of light for drug activation makes a drug with low dark toxicity generate cytotoxins electively within the cancerous tissues [1,2]. Due to the inherent advantages of photodynamic therapy including low levels of invasiveness and systematic toxicity, research in the area of photodynamic therapy has attracted considerable attention and a number of promising results have been demonstrated, including new molecules for the production of singlet oxygen ($^1O_2$) as well as transition metal complexes that covalently bind to DNA when photolyzed [3–5]. For instance, [Ru(bpy)(dppn)$(CH_3CN)_2]^{2+}$ (bpy = 2,2′-bipyridine, dppn = benzo[*i*]dipyrido-[3,2-a;2′,3′-c]phenazine) produced $^1O_2$ and dissociated ligand upon irradiation. Such dual reactivity has been proven to be a strategy for the improvement of the efficacy of phototherapeutic drugs by acting via two different mechanisms simultaneously [6].

In recent years, organometallic complexes has been widely investigated for their specific activities against different cancer cells, and favourable toxicity and clearance properties [7–9]. Among these complexes, the organometallic half-sandwish Ru(II) complexes have drawn increasing interest due to their great structural variety that provide the ability to fine-tune the chemical reactivity of the complexes. Sadler et al. have demonstrated the excellent cytotoxicity toward cancer cells of the complexes of the general structure $[(\eta^6$-arene)Ru(en)Cl$]^+$ (en = ethylenediamine) [10,11]. Dyson's group has reported the PTA complex, $[(\eta^6$-arene)Ru(PTA)$Cl_2]$ (PTA = 1,3,5-triaza-7-phosphatricyclo-[3.3.1.1]-decane), with activity against metastases [12,13]. Simultaneously, organometallic half-sandwish complexes derived from the neighboring group 9 members such as Rh(III) and Ir(III) have also been explored, and some complexes display high flexibility toward promising anticancer activity via intercalating target DNA in the cancer cells [14,15]. It has been believed that alteration of ligands about the metal center is an effective method to get complex with high activity, and a pronounced effect on biological activity can be achieved by fine

* Corresponding author.
E-mail address: lipearpear@163.com (P. Li).

https://doi.org/10.1016/j.pdpdt.2019.04.028
Received 28 March 2019; Received in revised form 22 April 2019; Accepted 26 April 2019
Available online 30 April 2019

tuning functional groups [16,17] However, there have been very few reports on half-sandwich complexes with dual activity of chemo- and phototherapeutic effect through the introduction of photosensitizer into the complexes, although the combination can embrace the advantages of the two different components and obtain synergistic anticancer effects. Juillerat-Jeanneret et al. have reported the first half-sandwich complex employed as photodynamic therapy agent. The coordination of Ru(II)-arene units to a porphyrin moiety results in efficient chemo- and phototherapeutic agents against human cancer cells, which is the combination of the photodynamic action of porphyrin with the cytotoxicity of Ru(II)-arene complexes [18,19]. Moreover, Wang et.al have reported the Ru(II)-arene complexes with a BODIPY (boron dipyrromethene)-modified pyridine ligand, in which the BODIPY ligand plays the photodynamic action, for photodynamic therapy application [20,21].

Our interest has focused on the development of efficient and selective half-sandwich complexes for anticancer agent. A vast number of novel Ru(II)-arene or pentamethylcyclopentadienyl (Cp*)- Rh(III) and Ir(III) complexes containing thiosemicarbazone ligands have been synthesized and evaluated for their antiproliferative activity [22–25]. Considering the potential advantages of combined chemo- and photodynamic therapy, herein we extended our study to the Cp*-Rh(III) and Cp*-Ir(III) complexes substituted with photosensitizers. The photosensitizers are anthracene derivatives, 9-anthraldehyde thiosemicarbazones (TSCs), which can generate $^1O_2$ both in vitro and in cells upon exposure to light and thus exhibit photodynamic activity [26] We surmise that the introduction of photosensitizer moiety can provide the resulting complexes with synergistic anticancer effects, by embracing the advantages of the different therapeutic mechanisms of the Cp*-Rh (III) and Cp*-Ir(III) complexes and photosensitizer. Bearing these in mind, a series of Cp*-Rh(III) and Cp*-Ir(III) complexes containing 9-anthraldehyde thiosemicarbazones were prepared and their photophysical properties and phototoxicity were investigated.

2. Experimental section

2.1. Materials and methods

$[(Cp^*)IrCl_2]_2$, $[(Cp^*)RhCl_2]_2$, thiosemicarabazide and other reagents were purchased from J&K Chemical Co. (China). All reagents and solvents were of high purity and used without further purification. All TSC ligands (L^1–L^2) were prepared using previously reported procedures [32]. NMR spectra were recorded with a Bruker AV-400 spectrometer at working frequencies 400 MHz and Bruker AV-600 spectrometer at working frequencies 600 MHz. Chemical shifts (δ) are expressed in parts per million and coupling constants (J) in hertz. Mass spectra for the complexes were recorded with a Waters UPLC XEVO G2 TOF mass spectrometer using electrospray ionization (ESI) probe. Elemental analyses were carried out using an Elementar Vario EL Cube. UV–vis absorption spectra were measured on a Cary 100 UV–vis spectrophotometer (Agilent Technologies, Inc., Australia). All fluorescence spectra were recorded on Thermo Scientific Lumina fluorescence spectrometer (Thermo Fisher Scientific, USA). The fluorescence quantum yields (Φ_F) were determined by following a previously reported method with rhodamine 6 G as the reference (Φ_F = 0.92 in DMF). The emission lifetimes were recorded with an Edinburgh Analytical Instruments FLS980 lifetime and steady-state spectrometer (405 nm picosecond pulsed laser and NIR PMT for Luminescence lifetime). Confocal fluorescence microscopy images were obtained using Nikon A1 confocal laser scanning microscope (Nikon, Japan).

Synthesis of (Cp*)Rh(L^1)Cl (1). $[(Cp^*)RhCl_2]_2$ (30.9 mg, 0.05 mmol), L^1 (28.3 mg, 0.1 mmol) were dissolved in 3 mL of ethanol. The reaction mixture was stirred at room temperature. After 4 h, the mixture was dried in vacuum, and gave a red solid that was further purified by recrystallization from dichloromethane and hexane. Yield: 32 mg, (51%). HR-ESI-MS (DMSO-d_6) m/z [Found (Calcd)]: 530.1152 (530.1137) (100%) $\{[(Cp^*)Rh(L^1)]^+ - Cl^- - H^+ \equiv [C_{27}H_{29}N_3SRh]^+\}$. IR ($cm^{-1}$): ν (NH_2, NH) 3432, 3252, 3190; ν (C = N) 1621; ν (C = S) 1045. ^{1}H NMR (600 MHz, CD_3Cl) δ, ppm 12.54 (br, 1H, N*H*), 10.30 (br, 1H, N*H*), 8.81 (s, 1H, -C*H*=N), 7.59–8.70 (m, 9H, anthryl-*H*), 2.98 (s, 3H, NHCH_3), 1.89 (s, 15H, -CH_3). Anal. Calcd for $C_{27}H_{30}N_3SClRh{\cdot}H_2O$: C, 52.05; H, 5.08; N, 6.56; Found: C, 52.55; H, 5.13; N, 6.76.

(Cp*)Rh(L^2)Cl (2). **2** was synthesized as for **1**. Yield: 32 mg, (51%). HR-ESI-MS (DMSO) m/z [Found (Calcd)]: 592.1306 (592.1294) (100%) $\{[(Cp^*)Rh(L^1)]^+ - Cl^- - H^+ \equiv [C_{32}H_{31}N_3SRh]^+\}$. IR ($cm^{-1}$): ν (NH_2, NH) 3445, 3253, 3149; ν (C = N) 1647; ν (C = S) 1050. ^{1}H NMR (400 MHz, DMSO-d_6) δ, ppm 9.28 (s, 1H, N*H*), 9.01 (s, 1H, N*H*), 8.72 (s, 1H, -C*H*=N), 7.45–8.69 (m, 9H, anthryl-*H*), 6.37–6.52 (m, 5H, phenyl-*H*), 1.83 (s, 15H, $-CH_3$). Anal. Calcd for $C_{32}H_{32}N_3SCl_2Rh{\cdot}1/2CH_2Cl_2$: C, 55.22; H, 4.70; N, 5.94; Found: C, 55.24; H, 4.71; N, 5.92.

(Cp*)Rh(L^3)Cl (3). **3** was synthesized as for **1**. Yield: 35 mg, (57%). HR-ESI-MS (DMSO) m/z [Found(Calcd)]: 620.1722 (620.1711) (100%) $\{[(Cp^*)Ir(L^1)]^+ - Cl^- - H^+ \equiv [C_{27}H_{29}N_3SIr]^+\}$. IR ($cm^{-1}$): ν (NH_2, NH) 3445, 3265, 3142; ν (C = N) 1647; ν (C = S) 1046. ^{1}H NMR (600 MHz, DMSO-d_6) δ, ppm 11.68 (br, 1H, N*H*), 9.25 (br, 1H, N*H*), 8.68 (s, 1H, -C*H*=N), 7.54–8.48 (m, 9H, anthryl-*H*), 2.98 (s, 3H, NHCH_3), 1.77 (s, 15H, -CH_3). Anal. Calcd for $C_{27}H_{30}N_3SCl_2Ir{\cdot}H_2O$: C, 45.69; H, 4.54; N, 5.92; Found: C, 45.91; H, 4.45; N, 5.87.

(Cp*)Rh(L^4)Cl (4). **4** was synthesized as for **1**. Yield: 29 mg, (43%). HR-ESI-MS (DMSO) m/z [Found (Calcd)]: 682.1864 (682.1868) (100%) $\{[(Cp^*)Ir(L^2)]^+ - Cl^- - H^+ \equiv [C_{32}H_{31}N_3SIr]^+\}$. IR ($cm^{-1}$): ν (NH_2, NH) 3445, 3147; ν (C = N) 1647; ν (C = S) 1051. ^{1}H NMR (600 MHz, DMSO-d_6) δ, ppm 9.26 (s, 1H, N*H*), 8.98 (s, 1H, N*H*), 8.69 (s, 1H, -C*H*=N), 7.42–8.37 (m, 9H, anthryl-*H*), 6.34–6.48 (m, 5H, phenyl-*H*), 1.79 (s, 15H, $-CH_3$). Anal. Calcd for $C_{32}H_{32}N_3SCl_2Ir{\cdot}3/4CH_2Cl_2$: C, 48.12; H, 4.13; N, 5.14; Found: C, 48.44; H, 4.07; N, 5.25.

2.2. X-ray crystallography

The reflection data was collected with a Bruker SMART CCD instrument using graphite monochromatic Mo Kα radiation (λ = 0.71073 Å) at room temperature. A semiempirical absorption correction using the SADABS program was applied, and the raw data frame integration was performed with SAINT. The crystal structures were solved by the direct method using the program SHELXS-97 [33] and refined by the full-matrix least-squares method on F^2 for all non-hydrogen atoms using SHELXTL-97 with anisotropic thermal parameters. All hydrogen atoms were located in calculated positions and refined isotropically, except the hydrogen atoms of water molecules that were fixed in a difference Fourier map and refined isotropically. The details of the crystal data are summarized in Table 1, and selected bond lengths and angles are listed in Table 2. Crystallographic data for the structural analysis have been deposited with the Cambridge Crystallographic Data Center (CCDC) with the following reference numbers: 1,857,695 and 1,857,697.

2.3. $^1O_2$ measurement

Measurements were taken at 420 nm excitation in air-saturated solutions at room temperature with TPP (Φ_Δ = 0.55, λ_{ex} = 400 nm) in $CHCl_3$ as references. The maximal absorption of the complexes at corresponding wavelength was generally kept between 0.01 and 0.3.

2.4. Phototoxicity

PC3 (human prostate carcinoma) and SKOV3 (human ovarian carcinoma) were obtained by Commerce. Photo and dark toxicity of the complexes were evaluated by WST-8 (water-soluble tetrazolium salts) assay using CCK-8 reagent. The cells (2 × 104 cells per well) were seeded on a 96-well plate in 200 μL of culture medium and incubated for 1 day at 37 °C in a 5% CO_2 atmosphere. Then 100 μL of micelle solutions prepared in culture medium at 5 μM complexes were added in

Table 1
Crystal data collection for **2** and **4**.

	$2{\cdot}CH_2Cl_2$	$4{\cdot}CH_2Cl_2$
formula	$C_{33}H_{34}Cl_4RhN_3S$	$C_{33}H_{34}Cl_4IrN_3S$
M_r	749.40	838.69
crystal system	monoclinic	monoclinic
space group	$P2_1/n$	$P2_1/n$
a (Å)	14.350(6)	14.401(3)
b (Å)	12.732(5)	12.792(3)
c (Å)	19.340(8)	19.188(4)
α (°)	90.00	90.00
β (°)	108.885(6)	108.445(3)
γ (°)	90.00	90.00
V (Å^3)	3343(2)	3353.2(13)
Z	4	4
D_c (Mg/m^3)	1.489	1.661
F (000)	1528	1656
μ (mm^1)	0.920	4.390
R_{int}	0.0323	0.0481
reflns collected	24167	36490
reflns ind	6109	6142
GOF (S)	1.055	1.061
R_1/wR_2 [I ≥ 2σ (I)]	0.0501/ 0.1396	0.0346/ 0.0869
R_1/wR_2 [all data]	0.0622/ 0.1511	0.0447/ 0.0944

Table 2
Selected bond lengths (Å), angles (deg) in **2** and **4.**

	2		**4**
Rh1-centroid	1.7967(5)	Ir1-centroid	1.7962(4)
Rh1-S1	2.3680(13)	Ir1-S1	2.3572(2)
Rh1-N1	2.1147(41)	Ir1-N1	2.1009(5)
Rh1-Cl1	2.4049(19)	Ir1-Cl1	2.3980(6)
N1-Rh1-S1	81.539(106)	N1-Ir1-S1	81.270(15)
N1-Rh1-Cl1	86.281(117)	N1-Ir1-Cl1	84.240(15)
S1-Rh1-Cl1	94.226(56)	S1-Ir1-Cl1	92.043(14)

each well. After 4 h incubation, the cells were exposed to a 300 W xenon lamp after passing through a color glass filter cut-on 400 nm for 30 min at the power density of 30 mW/cm [2], followed by 24 h incubation. Then 100 μL of fresh culture medium and 10 μL of CCK-8 reagent were added in each well and the cells were incubated for 3 h. Finally, the absorbance (A) at 450 nm was measured using a Thermo Scientific Multiskan MK3.

2.5. Confocal microscopic imaging

Confocal microscopy imaging of living cells Human SKOV3 cells were grown in a humidified at mosphere containing 5% CO_2 at 37 °C in DMEM medium supplemented with 10% FBS and 1% penicillin-streptomycin solution. SKOV3 cells were seeded onto 35 mm glass bottom culture dishes for 24 h after the concentration reached 5×10^5 cells/mL. Cells in exponential growth phase were used for experiment (2×10^4 cells/well) and seeded to 96-well plates for overnight. Then, the cells were incubated with the complexes (500 μg/mL) for another 4 h and then washed with phosphate buffered solution (pH 7.5) three times. Finally, the confocal microscopy imaging experiments were conducted (20 × objective).

3. Results

Figs. 1 and 2 shows the structures of complexes **2** and **4**. Tables 1 and 2 present their crystal data and selected bond lengths, angles. The photo- and chemocytotoxic effects of complexes **1–4** were investigated by means of the WST-8 assay in the human prostate carcinoma (PC3) and human ovarian carcinoma (SKOV3) cell lines (Figs. 6 and 7). In each case, cells were incubated with the complexes for 4 h in the absence of light, then subjected to light irradiation (λ_{irr} > 400 nm) for

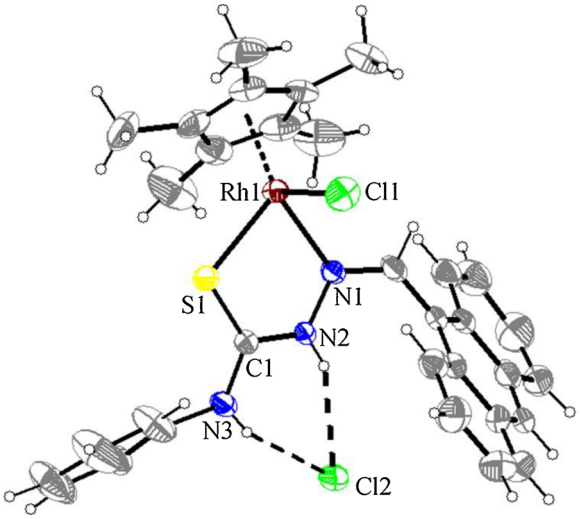

Fig. 1. ORTEP plots of **2**, the solvent molecules have been omitted for clarity.

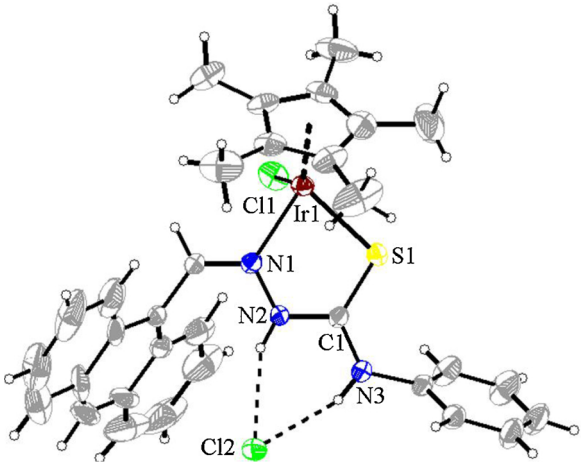

Fig. 2. ORTEP plots of **4**, the solvent molecules have been omitted for clarity.

30 min, and finally incubated in the dark for another 24 h. The complexes **1–4** exhibit moderate cytotoxicity against the two carcinoma cell lines in dark, with the IC_{50} values in the micromolar range (12.1–20.5 μM). Furthermore, after irradiation with light for 30 min, the IC_{50} values of **1–4** decrease to 2.3–8.7 μM.

4. Discussion

4.1. Synthesis and characterization

Complexes **1** and **2** were synthesized by stirring $[(Cp^*)RhCl_2]_2$ with the thiosemicarbazone ligands in a 2:1 mol ratio in ethanol at room temperature. Complexes **3** and **4** were prepared by reacting $[(Cp^*)IrCl_2]_2$ with the thiosemicarbazone ligands in ethanol at room temperature. The solids were recrystallized from dichloromethane and hexane (Scheme 1). The reaction produced red solids that were insoluble in acetone, $CHCl_3$, CH_2Cl_2 and DMSO. HR-ESI-MS, IR and 1H

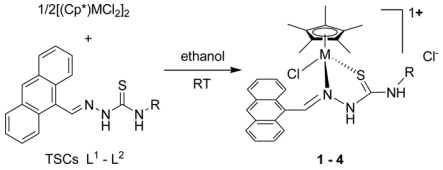

TSC	Complex	M	R
L^1	1	Rh	Me
L^2	2	Rh	Ph
L^1	3	Ir	Me
L^2	4	Ir	Ph

Scheme 1. Synthesis of the complexes **1–4**.

NMR spectral and elemental analyses were conducted for characterization of the complexes.

The X-ray crystal structures of a Cp*-Rh complex **2** and a Cp*-Ir complex **4** are presented in Figs. 1 and 2. The crystallographic data are shown in Table 1, and selected bond lengths and angles are listed in Table 2. In the molecular structures of the two complexes, Rh or Ir adopts the familiar 'three-legged piano-stool' geometry with the metal centre being coordinated by the aromatic Cp* ligand, a chelating N,S-ligand of 9-anthraldehyde thiosemicarbazone and a terminal chloride. The Cp* ligands are essentially planar, and the distances between the centroid of the Cp* ligand and the metal atoms are 1.7967(5) and 1.7962(4) Å, respectively. The bond distances around the metal atoms, Rh − S = 2.3680(13) Å, Rh − N = 2.1147(41) Å, Rh − Cl = 2.4049(19) Å in **2**, and Ir − S = 2.3572(2) Å, Ir − N = 2.1009(5) Å, Ir − Cl = 2.3980(6) Å in **4**; the bidentate angles around the metal atom, N1–Rh1–S1 [81.539(106)°], N1–Rh1–Cl1 [86.281(117)] and S1–Rh1–Cl1 [94.226(56)] in **2**, and N1–Ir1–S1 [81.270(15)°], N1–Ir1–Cl1 [84.240(15)] and S1–Ir1–Cl1 [92.043(14)] in **4**, are comparable to those of similar complexes.[24] The Cl component of the anion are interlinked by N2–H···Cl2 [2.3057(17) Å], N3–H···Cl2 [2.2277(18) Å] in **2** and N2–H···Cl2 [2.2963(8) Å], N3–H···Cl2 [2.2295(5) Å] in **4** via hydrogen bonding interactions.

4.2. Photophysical properties

The absorption and emission spectra of **1–4** in DMSO are shown in Fig. 3 and the basic photophysical properties of **1–4** are shown in Table 3. For these complexes, almost pure metal-to ligand charge transfer (^{1}MLCT) states are observed in the 350–300 nm region. The absorbance in the 350–450 nm region is mainly dominated by ligand and ^{1}MLCT transitions [27]. The complexes **1–4** exhibit the similar absorption spectra in which the absorption maximum is at 395 nm. Upon excitation at λ = 395 nm in the same solvent, the Cp*-Rh complexes **1**and **2** give emissions in λ = 514 and 517 nm, respectively, and the emissions of the corresponding Cp*-Ir Complexes **3** and **4** have a blue shift of ca. 20 nm with λ = 494 and 509 nm, respectively. The fluorescence quantum yields (Φ_F) of Cp*-Rh Complexes **1**and **2** are 0.038 and 0.044, respectively. Upon change to the Cp*-Ir moiety, the fluorescence quantum yields of both complexes **3** and **4** experience a marked increase, e.g. Φ_F = 0.077 and 0.049, respectively.

The singlet oxygen ($^1O_2$) quantum yields of complexes **1–4** were determined according to a previously reported method, using a steady-state method with 1,3-diphenylisobenzofuran (DPBF) as the quenching agent [28]. Taking tetraphenylporphyrin (H_2TPP) as the standard (Φ_Δ = 0.55 in $CHCl_3$),21 the $^1O_2$ quantum yields are measured to be 0.073 and 0.026 for the Cp*-Rh complexes **1** and **2**, respectively. Moreover, the Cp*-Ir complexes **3** and **4** produce singlet oxygen efficiently with values of 0.083 and 0.070, respectively (Table 3).

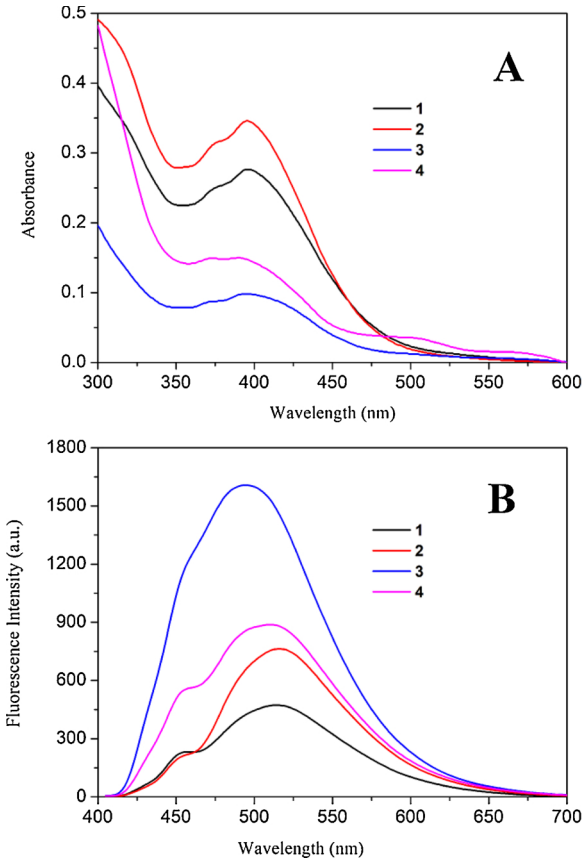

Fig. 3. UV–vis (A) and emission (B) spectra for **1–4** in DMSO.

Table 3
Electronic absorption and photophysical properties of **1-4**.

Complex	λ_{abs} (nm)	log ε	λ_{ex} [a](nm)	Φ_F [b]	[c]Φ_Δ
1	395	4.14	514	0.038	0.073
2	395	4.24	517	0.044	0.026
3	395	3.69	494	0.077	0.083
4	395	3.87	509	0.049	0.070

[a] Excited at 395 nm.
[b] Relative to rhodamine 6 G in DMSO as the reference (Φ_F = 0.92).
[c] Relative to H_2TPP in $CHCl_3$ as the reference (Φ_Δ = 0.55).

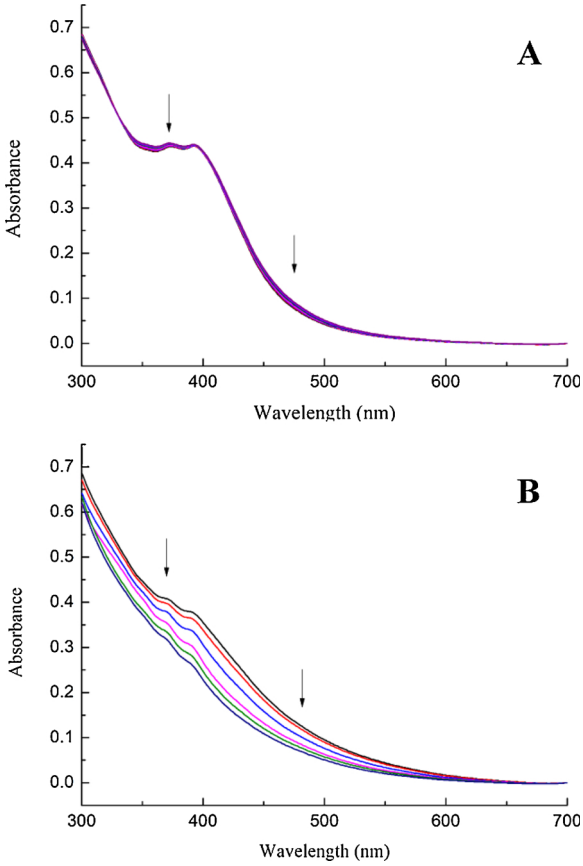

Fig. 4. Time-dependent UV-vis absorption spectra of **1** (10 μM) in DMSO–H_2O (A) for 30 min and (B) after irradiated 30 min, collected at 10, 20, 30, 70, 90, 180 min (λ > 400 nm).

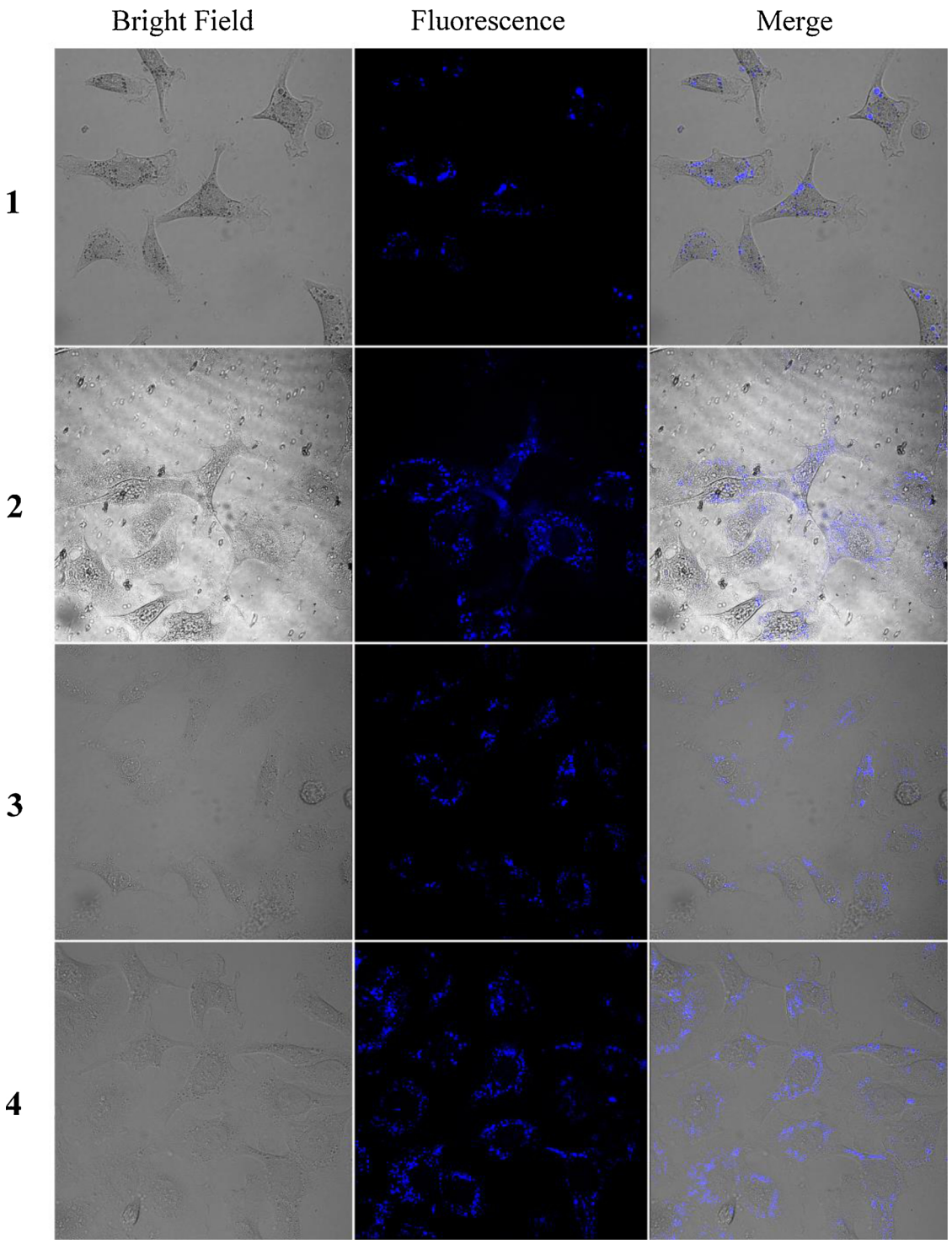

Fig. 5. Confocal fluorescence images of SKOV3 cells treated with complexes **1–4** for 4 h.

Since aqueous stability is important factor that affects the bioavailability of half-sandwish complexes, [29,30] the stability of complexes **1–4** were tested by monitoring their electronic absorption spectrum before and after irradiation. The complexes were dissolved in DMSO and subsequently diluted by water solution to give a final concentration of 1% (v/v) of DMSO. As shown in Fig. 4A, the time--dependent absorption spectra of **1** being monitored for 30 min, a slight decrease is observed for the intensity of the absorption bands of the complex between ~370 and ~470 nm. This change indicates the occurrence of slow hydrolysis, which is important in the biological functions of these complexes [31]. However, after light irradiation ($\lambda > 400$ nm) for 30 min, a stronger continued decrease is observed for the intensity of the absorption bands of the complex from ~370 to ~470 nm (Fig. 4B). Similar phenomenons are observed in the electronic absorption spectrum of **2–4** when the complexes are tested under similar experimental conditions (Supporting Information, Figures S1–S3), which suggests that the irradiation can obviously promote the hydrolysis of the complexes and shows positive affect on the improvement of their biological activity.

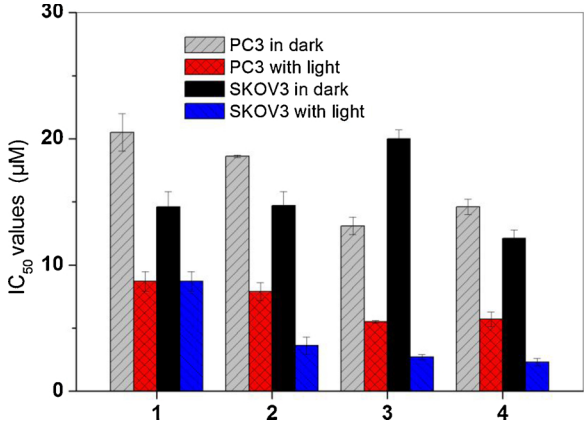

Fig. 6. IC_{50} values (μM) of complexes **1–4** against PC3 and SKOV3 cancer cell lines. $\lambda_{irr} > 400$ nm.

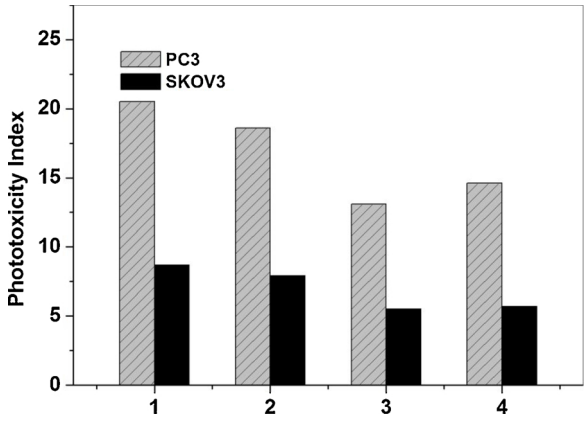

Fig. 7. Phototoxicity index [a] (PI) of complexes **1–4** against PC3 and SKOV3 cancer cell lines. $\lambda_{irr} > 400$ nm. [a] Dark IC_{50}/Light IC_{50}.

4.3. Cell uptake in vitro

In order to account for the different phototoxicity of these four complexes, their cellular uptake and subcellular localization were evaluated using intracellular fluorescence microscopy. As shown by the images captured by confocal laser scanning microscopy in Fig. 5, after SKOV3 cells are incubated with the complexes (10 μM) solution at 37 °C for 4 h, the blue fluorescence in cells is observed on 405 nm excitation. The merge of bright field and fluorescence images confirms that the complexes should be mainly located inside the cytoplasm without obvious nuclear uptake. The difference in fluorescence intensities is significant, with cells treated with **2** and **4** exhibiting much higher fluorescence intensities than those treated with **1** and **3**. The possible reason is that the N^4-phenyl on the thiosemicarbazone moiety of the complexes adjusts their lipophilicity and consequently results in an increased propensity to across the cell membranes [2,22].

5. Combined chemo- and photodynamic therapy studies in vitro

The WST-8 test was used for the comparison of the photosensitizers' efficiency. For comparison purposes, dark toxicity measurements were carried out in parallel. The complexes **1–4** exhibit moderate cytotoxicity against the two carcinoma cell lines in dark, with the IC_{50} values in the micromolar range (12.1–20.5 μM), which come from the intrinsic biological effect of these half-sandwish TSC complexes. Furthermore, after irradiation with light for 30 min, an increase in cell death is observed for samples dosed with all the complexes in both PC3 and SKOV3 cell lines (Fig. 6). Under the conditions tested here, the cytotoxicity towards PC3 cell lines of **1–4** increases approximately 2.5-fold in combination with light, with the IC_{50} values decrease to 5.5–8.7 μM. Cp*-Ir complex **3** is the most toxic complex when irradiated with light for 30 min, with IC_{50} of 5.5 μM, followed by **4** (IC_{50} = 5.7 μM) and then Cp*-Rh complex **2** (IC_{50} = 7.9 μM). Similarly, the phototoxicity enhancement of the four complexes toward SKOV3 cell lines under the present experimental conditions is observed. Cp*-Rh complexes **1** and **2** exhibit enhanced cytotoxicities upon irradiation with light, resulting in IC_{50} values of 8.7 and 3.6 μM, respectively, which is 1.7 and 4.1 times more cytotoxic than that in dark, respectively. Compared to Cp*-Rh complexes, Cp*-Ir complexes **3** and **4** exhibit high toxicity toward SKOV3 cell lines in the presence of light. The IC_{50} values of **3** and **4** with irradiation are 2.7 and 2.3 μM, respectively, which are up to 7.4 and 5.3 times more cytotoxic than that in dark, respectively. Although the phototoxicity of **3** is slightly lower than that of **4**, the phototoxicity index (PI) value for **3** is 1.4-fold greater than that for **4**, which indicates the effective PCT activity of the complex (Fig. 7).

It is reported that the half-sandwich analogues, Ru(II)-arene complexes containing BODIPY ligands, show good cytotoxicities under irradiation toward SKOV3 cell lines [21]. The PI values of these complexes are around 10, which is higher than those of **1–4.** However, compared with the first reported Cp*-Rh and Cp*-Ir complexes containing porphyrin for PDT application, which show poor phototoxicity, [18] the complexes **1–4** exhibit stronger phototoxicity, indicating that the introduction of anthracene derivatives seems to be an promising approach for the preparation of photosensitizer with potent photodynamic effects.

Cp*-Ir complexes **3** and **4** present more effective phototoxicity than Cp*-Rh complexes **1** and **2**. The possible reason is that Cp*-Ir complexes might induce DNA crosslinks or bind to proteins or other biomolecules in the cell following photoinduced biological effect. Noteworthily, although Cp*-Ir complex **3** shows not the highest uptake in these complexes, its higher $^1O_2$ quantum yield enables it to be more sensitive during light treatment, producing even greater phototoxic effect than the other complexes. Cp*-Rh complex **1** demonstrates modest phototoxicity under the conditions tested, which might due to the combined action of its low cellular uptake and medium $^1O_2$ quantum yield as well as the intrinsic biological effect of the Cp*-Rh complex.

6. Conclusions

In summary, a series of half-sandwich Cp*-Rh(III) and Cp*-Ir(III) complexes containing 9-anthraldehyde thiosemicarbazones (**1–4**) have been synthesized and characterized. The molecular structures of **2** and **4** have been characterized by X-ray crystallography. The complexes present a synergistic effect with good properties of both the Cp*-Rh(III) and Cp*-Ir(III) chemotherapeutic effect and the anthracene photodynamic therapy efficiency. Especially, Cp*-Ir(III) complexes **3** and **4** with remarkable phototoxic behavior in SKOV3 cancer cell lines (IC_{50} = 2.7 and 2.3 μM, respectively, $\lambda_{irr} > 400$ nm), along with the 7.4 and 5.3-fold lower toxicity in the dark, show potential as dual-action half-sandwish anticancer agents for combination therapy. This investigation demonstrates that the introduction of photosensitizer moiety into half-sanwish Cp*-Rh(III) and Cp*-Ir(III) complexes is an effective method for the design of a new generation of light activated dual-action anticancer agents.

Acknowledgements

This research was supported by the National Natural Science Foundation of China (21761006), Guangxi Natural Science Foundation (2016GXNSFCA380013, 2017GXNSFAA198335, 2018GXNSFAA281345), Guangxi Scientific and Technological Development Projects (AD17195081), "BAGUI Scholar" Program of Guangxi Province of China, Guangxi Key Laboratory of Natural Polymer Chemistry and Physics and Nanning Normal University, Natural Science Foundation of Guangxi

University of Chinese Medicine (2017JQ001), Natural Science Foundation of Team of Professor Shilin Yang (YSL17004).

Appendix A. Supplementary data

Supplementary material related to this article can be found, in the online version, at doi:https://doi.org/10.1016/j.pdpdt.2019.04.028.

References

[1] M. Ethirajan, Y. Chen, P. Joshi, R.K. Pandey, Chem. Soc. Rev. 40 (2011) 340–362.
[2] K. Mitra, S. Gautam, P. Kondaiah, A.R. Chakravarty, Angew. Chem. Int. Ed. 54 (2015) 13989–13993.
[3] W.A. Velema, W. Szymanski, B.L. Feringa, J. Am. Chem. Soc. 136 (2014) 2178–2191.
[4] M.A. Sgambellone, A. David, R.N. Garner, K.R. Dunbar, C. Turro, J. Am. Chem. Soc. 135 (2013) 11274–11282.
[5] M. Frasconi, Z. Liu, J. Lei, Y. Wu, E. Strekalova, D. Malin, M.W. Ambrogio, X. Chen, Y.Y. Botros, V.L. Cryns, J. Sauvage, J.F. Stoddart, J. Am. Chem. Soc. 135 (2013) 11603–11613.
[6] B.A. Albani, B. Peña, N.A. Leed, N.A.B.G. de Paula, C. Pavani, M.S. Baptista, K.R. Dunbar, C. Turro, J. Am. Chem. Soc. 136 (2014) 17095–17101.
[7] B.S. Murray, M.V. Babak, C.G. Hartinger, P.J. Dyson, Coord. Chem. Rev. 306 (2016) 86–114.
[8] J. Furrer, G. Süss-Fink, Coord. Chem. Rev. 309 (2016) 36–50.
[9] S. Mukhopadhyay, R.K. Gupta, R.P. Paitandi, N.K. Rana, G. Sharma, B. Koch, L.K. Rana, M.S. Hundal, D.S. Pandey, Organometallics 34 (2015) 4491–4506.
[10] R.E. Morris, R.E. Aird, Pdel S. Murdoch, H. Chen, J. Cummings, N.D. Hughes, S. Parsons, A. Parkin, G. Boyd, D.I. Jodrell, P.J. Sadler, J. Med. Chem. 44 (2001) 3616–3621.
[11] H. Chen, J.A. Parkinson, S. Parsons, R.A. Coxall, R.O. Gould, P.J. Sadler, J. Am. Chem. Soc. 124 (2002) 3064–3082.
[12] C. Scolaro, A. Bergamo, L. Brescacin, R. Delfino, M. Cocchietto, G. Laurenczy, T.J. Geldbach, G. Sava, P.J. Dyson, J. Med. Chem. 48 (2005) 4161–4171.
[13] S. Chatterjee, S. Kundu, A. Bhattacharyya, C.G. Hartinger, P.J. Dyson, JBIC J. Biol. Inorg. Chem. 13 (2008) 1149–1155.
[14] A. Petrini, R. Pettinari, F. Marchetti, C. Pettinari, B. Therrien, A. Galindo, R. Scopelliti, T. Riedel, P.J. Dyson, Inorg. Chem. 56 (2017) 13600–13612.
[15] J.P. Cerón-Carrasco, J. Ruiz, C. Vicente, C. de Haro, D. Bautista, J. Zúñiga, A. Requena, J. Chem. Theory Comput. 13 (2017) 3898–3910.
[16] M. Ali Nazif, J. – A. Bangert, I. Ott, R. Gust, R. Stoll, W.S. Sheldrick, J. Inorg. Biochem. 103 (2009) 1405–1414.
[17] Z. Liu, I. Romero-Canelón, A. Habtemariam, G.J. Clarkson, P.J. Sadler, Organometallics 33 (2014) 5324–5333.
[18] F. Schmitt, P. Govindaswamy, G. Süss-Fink, W.H. Ang, P.J. Dyson, L. Juillerat-Jeanneret, B. Therrien, J. Med. Chem. 51 (2008) 1811–1816.
[19] F. Schmitt, P. Govindaswamy, O. Zava, G. Süss-Fink, L. Juillerat-Jeanneret, B. Therrien, JIBC J. Biol. Inorg. Chem. 14 (2009) 101–109.
[20] Q.-X. Zhou, W.-H. Lei, Y.-J. Hou, Y.-J. Chen, C. Li, B.-W. Zhang, X.-S. Wang, Dalton Trans. 42 (2013) 2786–2791.
[21] T. Wang, Y. Hou, Y. Chen, K. Li, X. Cheng, Q. Zhou, X. Wang, Dalton Trans. 44 (2015) 12726–12734.
[22] W. Su, Q. Qian, P. Li, X. Lei, Q. Xiao, S. Huang, C. Huang, J. Cui, Inorg. Chem. 52 (2013) 12440–12449.
[23] W. Su, Z. Tang, P. Li, G. Wang, Q. Xiao, Y. Li, S. Huang, Y. Gu, Z. Lai, Y. Zhang, Dalton Trans. 45 (2016) 19329–19340.
[24] W. Su, B. Peng, P. Li, Q. Xiao, S. Huang, Y. Gu, Z. Lai, Appl. Organometal. Chem. 31 (2017) e3610.
[25] W. Su, Y. Li, B. Peng, J. Xie, P. Li, Q. Xiao, S. Huang, J. Organometal. Chem. 868 (2018) 24–30.
[26] D. Arian, L. Kovbasyuk, A. Mokhir, J. Am. Chem. Soc. 133 (2011) 3972–3980.
[27] W. Su, Q. Zhou, Y. Huang, Q. Huang, L. Huo, Q. Xiao, S. Huang, C. Huang, R. Chen, Q. Qian, L. Liu, Peiyuan Li, Appl. Organometal. Chem. 27 (2013) 307–312.
[28] X.-S. Ke, Y. Ning, J. Tang, J.-Y. Hu, H.-Y. Yin, G.-X. Wang, Z.-S. Yang, J. Jie, K. Liu, Z.-S. Meng, Z. Zhang, H. Su, C. Shu, J.-L. Zhang, Chem. Eur. J. 22 (2016) 9676–9686.
[29] R. Pettinari, F. Marchetti, F. Condello, C. Pettinari, G. Lupidi, R. Scopelliti, S. Mukhopadhyay, T. Riedel, P.J. Dyson, Organometallics 33 (2014) 3709–3715.
[30] P. Li, W. Su, X. Lei, Q. Xiao, S. Huang, Appl. Organometal. Chem. 31 (2017) e3685.
[31] H. Chen, J.A. Parkinson, S. Parsons, R.A. Coxall, R.O. Gould, P.J. Sadler, J. Am. Chem. Soc. 124 (2002) 3064–3082.
[32] F.A. Beckford, G. Leblanc, J. Thessing, M. Shaloski Jr, B.J. Frost, L. Li, N.P. Seeram, Inorg. Chem. Commun. 12 (2009) 1094–1098.
[33] G.M. Sheldrick, Acta Crystallogr. A 46 (1990) 467.